The Predicted Structures of the New Pnictides HfMQ in Contrast to ZrMQ (M = Ti, V; Q = P, As)

Shahab Derakhshan,[a] Enkhtsetseg Dashjav,[a] and Holger Kleinke*[a]

Keywords: Structure map / X-ray diffraction / Electronic structure / Phosphides / Arsenides

The new pnictides HfTiP, HfTiAs and HfVAs have been prepared through arc-melting. These arsenides form the predicted structures with (distorted) $TiAs_4$ and VAs_4 tetrahedra, while the structures of both Zr analogs (ZrTiAs and ZrVAs) are comprised of $TiAs_4$ and VAs_4 square planes, respectively. These differences stem from significant differences in the metal atom substructures. On the other hand, HfTiP and ZrTiP are isostructural. These variations were predicted by utilizing a structure map for metal-rich pnictides and chalcogenides M_2Q (M = valence-electron poor transition metal, Q = pnicogen or chalcogen) presented in the year 2000. The HfMQ structure is stabilized by strong Hf–Q, M–Q and M–M bonds, and to a minor extent by Hf–Hf and Hf–M bonding interactions. All three new $Hf_{1-\delta}M_{1+\delta}Q$ phases exhibit significant phase ranges.

Introduction

The ternary equiatomic early transition-metal pnictides MM′Q (M, M′: element of groups 3−5; Q: P, As, Sb) typically occur in one of two common crystal structures. These structures differ in the metal−nonmetal coordination spheres (but with the same coordination numbers) as well as in the metal−metal bonding, while the nonmetal atoms are always surrounded by nine metal atoms in form of a tricapped trigonal prism, and the larger M atoms are situated in a square pyramid formed by five Q atoms. In the first variant, the Co_2Si type (ordered variant: TiNiSi[1]), the smaller M′ atoms are tetrahedrally coordinated by four Q atoms, whereas in the second variant, the La_2Sb type (ordered variant: CeScSi[2]), the $M'Q_4$ polyhedra are best described as square planes.

These differences may be understood to stem from different metal atom substructures, which contain stronger M−M and M−M′ bonds in case of the Co_2Si structures. As shown earlier,[3] the major structure determining factors for such metal-rich pnictides and chalcogenides are the valence-electron concentration of M, the relative extension of the d orbitals of M (reflected in the principal quantum number), the radius ratio r_M/r_Q, and the electron deficit of the Q atoms. As for the metal atoms, higher valence-electron concentration, larger d orbitals and larger atomic radii all facilitate stronger M−M bonding. On the other hand, larger atomic sizes and larger electron deficits of the Q atoms would lead to larger coordination numbers for the Q atoms. Given the fact that the known structure types all have comparable packing efficiencies, more M−M bonds occur with smaller coordination numbers of the Q atoms. Obviously these factors can cancel each other, one example being Zr_2S and Hf_2P that are isostructural.

All these factors were summarized empirically in the power product $\mathbf{f} = vec_M \times n_M^2 \times (r_M/r_Q)/(8 - e_Q)^2$, wherein vec_M equals the valence-electron concentration per M atom after (formally) reducing the Q atoms, n_M the main quantum number of the M atoms, (r_M/r_Q) the radius ratios based on the Slater radii,[4] and $(8 - e_Q)$ the electron deficit of the Q atoms in their neutral state − in analogy to the $(8 - N)$ rule. Plotting the averaged coordination number of the Q atoms <C.N.(Q)> of all M_2Q pnictides and chalcogenides, including the ternaries with two different M atoms as well as two different Q atoms, against **f** gave a structure map with distinct domains of the (then) eleven different structure types of this family.[3]

For all of the factors contributing to the power product **f** are readily available, **f** may be calculated for all hypothetical, still uncovered M_2Q binaries as well as $M_{1-\delta}M'_{1+\delta}Q$ and $M_2Q_{1-\delta}Q'_\delta$ ternaries. Then, the domain and thus the structure type can be predicted, unless the compound in question either does not exist or forms a new type. However, unlike well-known structure maps such as Pettifor's[5] or Villars',[6] this approach even suggests information about unknown types, namely the averaged coordination number of the Q atoms.

The (in part systematic) subsequent recovery of new members of this M_2Q family proved the usability of this structure map: the ternary arsenide, $Zr_{1-\delta}Ti_{1+\delta}As$, was postulated to form the La_2Sb type, which was subsequently proven to be correct.[7] $Zr_{1-\delta}V_{1+\delta}As$[8] is at the border be-

[a] Department of Chemistry, University of Waterloo
Waterloo, Ontario, Canada N2 L 3G1
Fax: (internat.) +1-519-746-0435
E-mail: kleinke@uwaterloo.ca

tween the Co_2Si and La_2Sb representatives of this family, depending on the exact Zr:V ratio, and always forms the La_2Sb structure. Harbrecht et al. uncovered with Zr_6STe_2 ($\equiv Zr_2S_{0.33}Te_{0.67}$)[9] the first example of a new compound in this family that occurs in a new type, and its <C.N.(Q)> value is indeed eight − thus a nice fit in the structure map. Furthermore, an extension to other stoichiometries is possible, as demonstrated by us for the M_5Q_3 compounds.[10,11]

This work deals with the new hafnium phosphides and arsenides $Hf_{1-\delta}Ti_{1+\delta}P$, $Hf_{1-\delta}Ti_{1+\delta}As$, and $Hf_{1-\delta}V_{1+\delta}As$. As illustrated in Table 1, the power product **f** clearly places these three new materials into the Co_2Si domain, together with ZrTiP,[12] ZrVP and HfVP,[13] ZrNbP and HfNbP,[14] and V_2P[15] and in contrast to ZrTiAs and ZrVAs (as well as La_2Sb[16] and Zr_2Sb[17]). Our investigations confirmed the Co_2Si type in all three new cases introduced.

Table 1. Overview of M_2Q compounds in the Co_2Si and La_2Sb types. Hypothetical compounds are in italic

Compound	f	Structure	Reference
HfNbP	15.1	Co_2Si	[14]
TaVP	13.6	Co_2Si	[12]
ZrNbP	12.5	Co_2Si	[14]
HfVP	12.1	Co_2Si	[13]
HfVAs	10.5	Co_2Si	this work
HfTiP	10.2	Co_2Si	this work
ZrVP	9.8	Co_2Si	[13]
HfTiAs	8.9	Co_2Si	this work
V_2P	8.4	Co_2Si	[15]
ZrTiP	8.3	Co_2Si	[12]
ZrVAs	8.5	La_2Sb	[8]
La_2Sb	8.1	La_2Sb	[16]
Zr_2Sb	7.4	La_2Sb	[17]
ZrTiAs	7.2	La_2Sb	[7]
HfTiSb	7.1	predicted La_2Sb	hypothetical
ZrTiSb	5.7	predicted La_2Sb	hypothetical

Results and Discussion

Structure Map

Several ternary phosphides, arsenides and antimonides of Zr and Hf form the Co_2Si type. Typically, the second metal is a late transition-metal atom, as in ZrMP (M = Fe, Co),[18,19] HfMP (M = Fe, Co, Ni),[20] ZrMAs and HfMAs (M = Fe, Co, Ni),[21] and ZrMSb and HfMSb (M = Fe, Ni).[22,23] With the exception of ZrNiP (Ni_2In type)[24] and HfNiP, these Zr and Hf compounds are always isostructural. Only few examples are known with Zr or Hf and a second early transition metal, namely the phosphides ZrTiP,[12] ZrVP and HfVP,[13] ZrNbP and HfNbP[14] (all Co_2Si type), while the arsenides known to date form the La_2Sb type (i.e. ZrTiAs and ZrVAs[7,8]). Furthermore, no such antimonides were uncovered to date.

Employing the structure map for M_2Q compounds, the hitherto unknown pnictides HfTiP, HfTiAs and HfVAs were predicted to form the Co_2Si type (cf. the overview in Table 1).[7,8] Our investigations presented here prove this to be correct. Knowledge of the structures of related pnictides published before could not be used for this prediction, as ZrTiAs and ZrVAs both occur only in the La_2Sb type, while ZrTiP crystallizes (like HfTiP) in the Co_2Si type.

In particular, one might have correctly assumed HfTiP to be isostructural with ZrTiP, but following this logic, HfTiAs should be isostructural with ZrTiAs, which is not the case. A thorough theoretical investigation of ternary phosphides MM′P, with M and M′ being an early transition-metal element,[25] was based on Extended Hückel calculations,[26,27] using the atomic parameters of Zr and Nb. This work analyzed four different possible structure types, namely Cu_2Sb, Co_2Si, Fe_2P and Ni_2In. For 14 valence-electrons, the Co_2Si type was calculated to be electronically preferred, which is the case for MNbP, MVP and MVAs with M = Zr, Hf. Similar compounds with 13 valence-electrons − explicitly mentioned was HfTiP in that article − were predicted to form the Cu_2Sb type, which exhibits a M atom substructure related to that of the La_2Sb type. To summarize, the latter method, which exclusively used valence-electron concentrations for rationalizing structural trends, correctly identified ZrVP, HfVP and HfVAs, but failed to foresee correctly ZrTiAs, ZrVAs, HfTiP and HfTiAs.

Crystal Structure

Since the Co_2Si type (*anti*-$PbCl_2$) is a well-known structure type, its description may be kept short here. We are therefore concentrating on the differences to the La_2Sb type, for ZrTiAs and ZrVAs adopt the latter, and HfTiAs and HfVAs the former type. In the following, we will discuss the differences between HfVAs and ZrVAs, whose structures are shown in Figure 1.

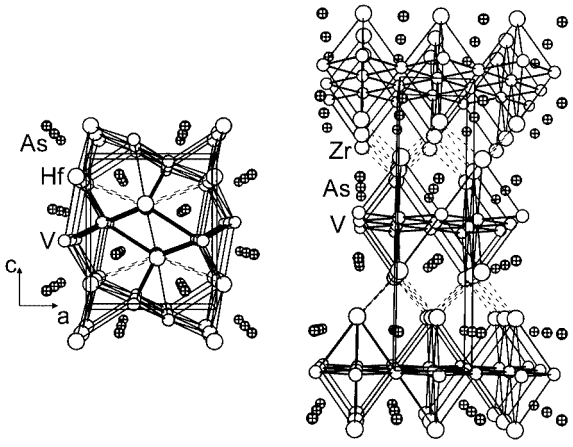

Figure 1. Crystal structures of HfVAs (left) and ZrVAs (right)

Both structures comprise three atomic positions, one As, one M(1) (mainly the group 4 element, i.e. Zr or Hf) and one M(2) (mainly V) site. Depending on the exact M:V ratio of $Zr_{1-\delta}V_{1+\delta}As$ and $Hf_{1-\delta}V_{1+\delta}As$, the M(1) site may exhibit up to 15% V in ZrVAs and 9% V in HfVAs, and the M(2) site up to 43% Zr in ZrVAs and 2% Hf in HfVAs. It is noted that in the case of MTiAs, the M(2) site cannot

include any Zr of Hf contributions, but M(1) up to 42% Ti in ZrTiAs and 40% Ti in HfTiAs.

In both structures, ZrVAs and HfVAs, the As atom is surrounded by nine transition-metal atoms forming a (distorted) tri-capped trigonal prism (deltahedral tetrakaidecahedron), namely five M(1) and four M(2) atoms. Furthermore, the M(1) atoms are located in (distorted) As_5 square pyramids in both structures, but the V atom in a (distorted) As_4 tetrahedron in HfVAs and in an As_4 planar "square" (more precisely: rectangle) in ZrVAs. These coordination polyhedra are depicted in Figure 2.

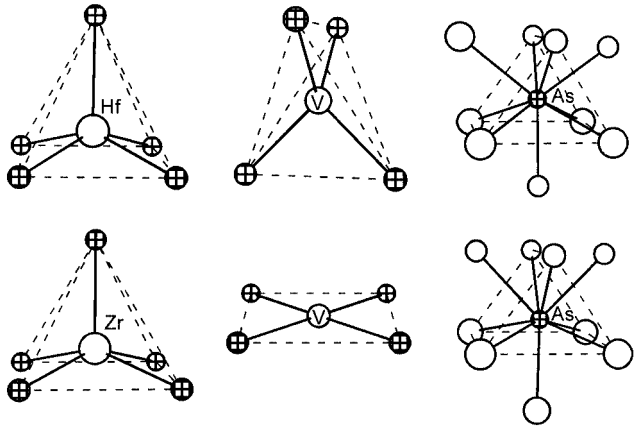

Figure 2. Coordination polyhedra of HfVAs (top) and ZrVAs (bottom)

The different coordination numbers of M(1) and M(2) reflect a likely reason why the smaller V atom prefers the M(2) site in both cases. As well, the coordination number of four inhibits an incorporation of the group 4 element to some extent; only in the case of ZrVAs may the M(2) site exhibit significant amounts of it.

Of particular interest are the differences in metal−metal bonding in these structures, for the only (yet obvious) difference between the formulas ZrVAs and HfVAs is the main quantum number of the group 4 metal atoms. Size and electronegativity of Zr and Hf atoms are virtually equivalent. ZrVAs comprises sheets of corner-sharing Zr_2V_4 octahedra (tetragonally elongated, i.e. of D_{4h} symmetry), wherein the apices are occupied by Zr atoms. Then, the V atoms form planar square nets, whose interatomic distances are much shorter than the Zr−V distances, namely 268 pm vs. 326 pm in $Zr_{0.85}V_{1.15}As$ (each 4 × per V atom). Additional M−M bonding occurs between the sheets of octahedra in form of Zr−Zr bonds of 341 pm.

More complex, and truly three-dimensional, is the bonding situation in HfVAs. V−V zigzag chains with short interatomic distances of 266 pm (in $Hf_{0.97}V_{1.03}As$) run along the *b* axis. While that bond length is similar to the V−V bonds in ZrVAs, the multitude is smaller, with two bonds per V atom in HfVAs, compared to four bonds per V atom in ZrVAs. Each V atom in HfVAs is additionally connected to Hf atoms at rather short distances of 2 × 298 pm and 2 × 308 pm, and longer ones of 321 pm and 334 pm. The Hf−Hf distances vary between 329 pm and 363 pm.

The four Hf−V distances between 298 pm and 308 pm and the six Hf−Hf between 329 and 363 pm stand against the four Zr−V at 326 pm and four Zr−Zr distances at 340 pm of ZrVAs. It is evident that the Hf atoms in HfVAs participate in more and shorter M−M bonds than the Zr atoms in ZrVAs. Remembering that the radii of the Zr and Hf atoms are virtually equivalent (e.g., Slater radii: 155 pm for both atoms, Pauling's single bond radii: 145 pm for Zr and 144 pm for Hf[28]), the reason behind this cannot be of steric nature. Since the relative extension of the *d* orbitals is higher in case of the *5d* elements, they principally tend to form more and stronger M−M bonds than the *4d* elements. This fact was used to explain the site preferences of the Ta atoms in ternary niobium tantalum sulfides,[29,30] as well as the differences between the structures of ZrNiP and HfNiP.[20] Similarly, the different main quantum numbers of Zr and Hf led to the different power factors **f** of ZrVAs and HfVAs, which ultimately results in the occurrence in different structure domains in our structure map, namely the La_2Sb and Co_2Si domains, respectively.

The differences in bond lengths (Table 2) between $Hf_{0.97}V_{1.03}As$ and $Hf_{0.92}V_{1.08}As$ stem from size differences between Hf and V (Slater radius of V: 135 pm). The same is true for $Hf_{0.84}Ti_{1.16}As$ and $Hf_{0.60}Ti_{1.40}As$. Although the latter two compounds are less Hf-rich, their unit cell volumes and bond lengths are larger than those of the V compounds, because of the larger size of Ti, compared to V (140 pm vs. 135 pm).

Table 2. Selected interatomic distances [pm]

Bond	No.	*d*[a]	*d*[b]	*d*[c]	*d*[d]
M(1)−As	2 ×	273.6(2)	272.0(1)	271.7(2)	269.9(1)
M(1)−As	2 ×	278.2(2)	277.5(1)	273.3(2)	271.3(1)
M(1)−As	1 ×	294.5(2)	292.4(2)	286.2(3)	284.9(1)
M(1)−M(1)	2 ×	335.3(2)	334.9(2)	329.2(2)	327.70(9)
M(1)−M(1)	2 ×	361.34(7)	360.41(8)	358.88(9)	357.06(6)
M(1)−M(1)	2 ×	369.6(2)	367.4(2)	362.7(2)	360.1(2)
M(1)−M(2)	2 ×	299.5(2)	297.8(2)	298.3(3)	296.2(2)
M(1)−M(2)	2 ×	315.2(3)	313.8(2)	308.1(3)	306.0(2)
M(1)−M(2)	1 ×	333.2(3)	331.9(2)	320.6(3)	318.5(2)
M(1)−M(2)	1 ×	336.9(3)	336.2(2)	333.8(3)	331.6(2)
M(2)−As	2 ×	257.3(3)	256.8(2)	252.0(3)	251.01(2)
M(2)−As	1 ×	263.0(4)	261.7(3)	259.6(4)	257.5(2)
M(2)−As	1 ×	267.0(4)	266.5(3)	258.4(4)	256.9(2)
M(2)−M(2)	2 ×	275.3(4)	274.4(4)	265.9(5)	265.1(3)

[a] $Hf_{0.84(1)}Ti_{1.16}As$. [b] $Hf_{0.602(5)}Ti_{1.40}As$. [c] $Hf_{0.97(2)}V_{1.03}As$. [d] $Hf_{0.916(6)}V_{1.084}As$.

Mixed Occupancies

All four structures analyzed here exhibit mixed occupancies on at least one metal atom site, that is, Hf/Ti and Hf/V mixtures. The same is true for $Zr_{0.58}Ti_{1.42}As$, $Zr_{1.43}V_{0.57}As$ and $Zr_{0.85}V_{1.15}As$, but not for ZrTiAs at the exact 1:1 ratio of Zr:Ti. The latter indicates a strong preference for ordering, for the two available atom sites as well as atom kinds are quite different. Hf/Ti mixed occupancies were observed in $(Hf,Ti)_7Sb_4$ [31] with almost no differences

between the metal atom sites, and Zr/V and Zr/Ti mixed occupancies with intermediate ordering in $(Zr,V)_{13}Sb_{10}$,[32] $(Zr,V)_{11}Sb_8$,[33] and (Zr,Ti)Sb.[34] All of these observations may be explained with the various extents of the differences between the metal atom sites of the respective structures.

Electronic Structure

To further characterize HfMAs and to gain more insight into the differences between ZrMAs and HfMAs, we analyze the band structures of HfTiAs and HfVAs, as ZrVAs and ZrTiAs were investigated before. The Densities Of States (DOS) and selected Crystal Orbital Hamilton Populations (COHP)[35] curves, each cumulated over the whole unit cell, are shown in Figure 3 (HfTiAs) and Figure 4 (HfVAs). The facts, that the structures are isotypic and the constituent elements similar, are reflected in comparable, yet not equivalent, shapes of the DOS curves. As a consequence of the different valence-electron concentration, due to Ti being a 4th and V a 5th group element, the DOS of HfVAs is shifted up by more than 0.5 eV with respect to HfTiAs, with both Fermi levels fixed at 0 eV. In both cases, the energy windows shown exclude the As-*s* dominated peak, which occurs well below −7 eV. A pseudo gap (at −2.0 eV in the Ti and −2.7 eV in the V case) separates the As-*p* peak from the metal-centered states.

Hf, Ti and V contributions below −2.0 eV and −2.7 eV, respectively, are indicative of covalent M−As bonding character. As may be seen in the COHP curves on the right sides of the Figure 3 and 4, all M−As interactions are strong, and only bonding states are filled. Virtually no M−As states are found in the vicinity of the Fermi level. The same statements can be made in the cases of ZrTiAs and ZrVAs.

A second pseudo gap is located within the M-*d* peak, separating bonding M(2)−M(2) interactions from the antibonding ones. The Fermi level is found slightly below this local minimum in HfTiAs, and slightly above it in HfVAs. In both cases the Fermi level is located in the midst of the metal *d* states, emphasizing the importance of the *d* states for the bonding and thus crystal structure. The V−V bonds are optimized in HfVAs, that is, the transition from bonding to antibonding character takes place directly at the Fermi level. The Ti−Ti bonds in HfTiAs would gain bonding character by an increase of valence-electrons, because empty bonding states are found up to 1 eV above the Fermi level.

That Hf is the most electropositive element here, and thus the higher oxidized M atom, reflects itself in fewer filled Hf−Hf bonding states, compared to both Ti−Ti and V−V states. Therefore, the Hf−Hf interactions are less dominant,

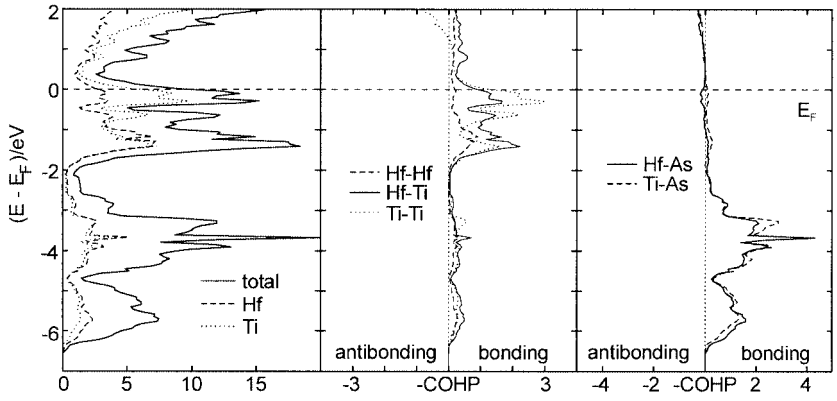

Figure 3. Densities of states (left) and selected cumulated COHP curves for HfTiAs

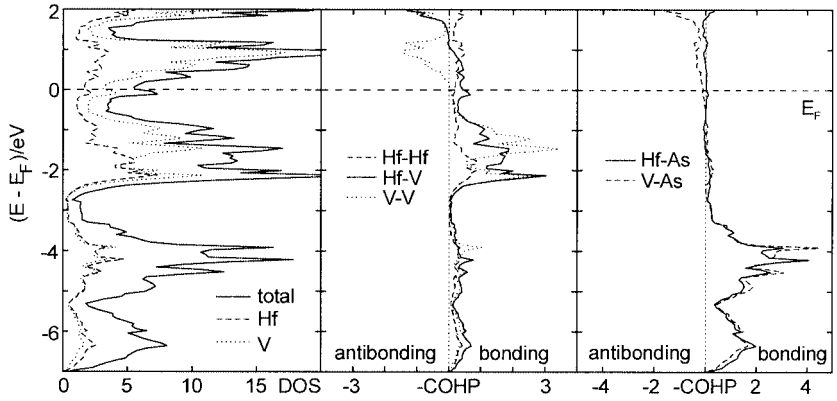

Figure 4. Densities of states (left) and selected cumulated COHP curves for HfVAs

and they exhibit exclusively bonding states within the depicted energy window. The latter is also true for the Hf−Ti interactions in HfTiAs, but not for the Hf−V interactions in HfVAs. The latter turn into antibonding character about 1 eV above the Fermi level.

The most striking difference between the M−M COHP curves of the Zr and Hf arsenides under consideration is the relative importance of the Ti−Ti and V−V interactions, in relation to the other kinds. While they seem to be the strongest in all cases, they are less dominant in the Hf cases, particularly compared to the Hf−Ti and Hf−V bonds, respectively. In turn, the Hf−M′ bonds are thus more important in the HfM′As structures than the Zr−M′ bonds in ZrM′As. This observation is in tune with the assumption that Hf may form stronger metal−metal bonds than Zr because of the larger extension of its *5d* orbitals, as all the metal−metal interactions rely almost exclusively on the *d* states.

Conclusion

Three new compounds, all with significant phase ranges, have been introduced: $Hf_{1-\delta}Ti_{1+\delta}P$, $Hf_{1-\delta}Ti_{1+\delta}As$, and $Hf_{1-\delta}V_{1+\delta}As$, all crystallizing in the Co_2Si type. This completes the series of ternary Zr/Hf − Ti/V phosphides and arsenides that form either the Co_2Si or the La_2Sb type. Evidently all these compounds fit into the recently published M_2Q structure map based on the power product $\mathbf{f} = vec_M \times n_M^2 \times (r_M/r_Q)/(8 - e_Q)^2$ − higher **f** values are indicative of more M−M bonding. On the other hand, electron counting or basic analogy considerations failed to explain the respective crystal structures, as for both structure variants examples exist with 13 as well as 14 valence-electrons, and seemingly analogous compounds such as ZrTiAs and HfTiAs occur in different types, while ZrTiP and HfTiP are isostructural.

While all kinds of M−M bonding occur in both types, the Hf−Hf and Hf−Ti/V bonds of HfTiAs and HfVAs are shorter than the respective Zr-containing bonds in ZrTiAs and ZrVAs (the latter both La_2Sb type). That difference may be understood based on the different main quantum numbers n_{Zr} and n_{Hf}, considering that higher quantum numbers enable the metal atom to form stronger M−M bonds (cf. n_M in the power product **f**).

Experimental Section

Syntheses of HfMP and HfMAs

All experiments started from the elements as purchased in microcrystalline form from Aldrich, with purities above 99.5%. The first steps were the syntheses of the monopnictides HfP, HfAs, TiP, TiAs, and VAs as starting materials, which were necessary to minimize mass losses due to vaporization of phosphorus or arsenic during arc-melting and tube attacks during annealing in tantalum containers, respectively. The monoarsenides were prepared starting from the elements in the stoichiometric 1:1 ratios in evacuated fused silica tubes at 800 °C, and TiP was synthesized at 400 °C under addition of trace amounts of iodine. Then, more metal was added to reach the target ratio of metal/pnicogen of 2:1. These mixtures were thoroughly ground, pressed into pellets and then arc-melted twice under a flow of Argon. This procedure led to the synthesis of HfTiP, HfTiAs and HfVAs in yields of 80−90%, as estimated based on the powder diagrams obtained using an X-ray powder diffractometer with position-sensitive detector (Inel). Higher yields were obtained in the HfTiP system by annealing the mixtures in sealed tantalum containers at 1400 °C over a period of several days (without prior arc-melting).

Phase Ranges of $Hf_{1-\delta}Ti_{1+\delta}P$ and $Hf_{1-\delta}M_{1+\delta}As$

$Zr_{1-\delta}Ti_{1+\delta}As$ and $Zr_{1-\delta}V_{1+\delta}As$ (both La_2Sb type) exhibit significant phase ranges, with $0 \le \delta \le 0.42(1)$ and $-0.43(4) \le \delta \le 0.15(1)$, respectively.[7,8] $Zr_{1-\delta}V_{1+\delta}P$ and $Hf_{1-\delta}V_{1+\delta}P$ (both Co_2Si type) were reported to have significant phase widths as well ($0 \le \delta \le 0.40$ and $0 \le \delta \le 0.55$).[13] Therefore, we varied the Hf:M ratios to determine the phase ranges of $Hf_{1-\delta}Ti_{1+\delta}P$ and $Hf_{1-\delta}M_{1+\delta}As$. These investigations were started with arc-melting different mixtures in the arsenic system:

$HfAs + Ti \rightarrow Hf_{1-\delta}Ti_{1+\delta}As + Hf_3As + ?$ (**I**)

$0.75\ Hf + 0.25\ Ti + TiAs \rightarrow Hf_{1-\delta}Ti_{1+\delta}As + ?$ (**II**)

$0.5\ Hf + 0.5\ Ti + TiAs \rightarrow Hf_{1-\delta}Ti_{1+\delta}As + Ti_3As + ?$ (**III**)

$0.25\ Hf + HfAs + 0.75\ V \rightarrow Hf_{1-\delta}V_{1+\delta}As + Hf_3As + ?$ (**IV**)

$HfAs + V \rightarrow Hf_{1-\delta}V_{1+\delta}As + ?$(**V**)

$0.75\ Hf + 0.25\ V + VAs \rightarrow Hf_{1-\delta}V_{1+\delta}As + V_3As + ?$ (**VI**)

The products of the reactions (**I**) − (**VI**), as determined by X-ray powder diffraction, indicate different phase ranges for the Ti- and V-containing Hf arsenides, namely $0 < \delta < 0.5$ for $Hf_{1-\delta}Ti_{1+\delta}As$ and $-0.25 < \delta < 0.25$ for $Hf_{1-\delta}V_{1+\delta}As$. The symbol "?" implies the presence of unidentified compounds in small yields.

Analogous investigations in the Hf−Ti−P system were carried out at 1400 °C, for arc-melting proved to be more difficult, most likely due to phosphorus vaporization. Reactions aiming at $Hf_{1-\delta}Ti_{1+\delta}P$ were carried out with δ varying between −0.5 and +0.5, and $Hf_{1-\delta}Ti_{1+\delta}P$ was formed as the main product when $-0.2 \le \delta \le 0.5$. The lattice dimensions of the Co_2Si type phases were determined from their X-ray powder diagrams by least-square refinements (assuming orthorhombic symmetry). EDS analyses (LEO, 1530, with integrated EDAX Pegasus 1200) on several selected crystals of the Co_2Si phases did not reveal any incorporation of impurity elements, such as Si or oxygen stemming from the silica tube or Ta coming from the tantalum container, or iodine from the synthesis of TiP. According to the averaged values of these analyses (summarized in Table 3), $Hf_{1-\delta}Ti_{1+\delta}P$ exists between $Hf_{0.6}Ti_{1.4}P$ and $Hf_{1.2}Ti_{0.8}P$ (i.e. $-0.2 \le \delta \le 0.4$). An increasing Hf content is reflected in larger cell volumes, for Hf atoms are larger than Ti atoms (e.g., Slater radii: 155 pm vs. 140 pm).

Table 3. Lattice dimensions of powdered HfTiP samples and EDX results of selected crystals thereof

Target	EDX	*a*/pm	*b*/pm	*c*/pm	*V*/nm³
"$Hf_{0.5}Ti_{1.5}P$"	$Hf_{0.61}Ti_{1.39}P$	661.4(7)	350.8(3)	803.7(9)	0.1865(6)
"$Hf_{0.6}Ti_{1.4}P$"	$Hf_{0.58}Ti_{1.42}P$	662.9(4)	351.3(2)	805.8(6)	0.1877(4)
"$Hf_{0.7}Ti_{1.3}P$"	$Hf_{0.80}Ti_{1.20}P$	665.7(5)	352.3(2)	807.6(6)	0.1894(4)
"$Hf_{0.8}Ti_{1.2}P$"	$Hf_{0.80}Ti_{1.20}P$	668.0(5)	354.0(4)	809.4(8)	0.1914(6)
"$Hf_{0.9}Ti_{1.1}P$"	$Hf_{0.87}Ti_{1.13}P$	668.5(6)	354.6(4)	810.3(6)	0.1921(5)
"HfTiP"	$Hf_{1.03}Ti_{0.97}P$	670.5(5)	354.8(2)	812.4(6)	0.1933(4)
"$Hf_{1.1}Ti_{0.9}P$"	$Hf_{1.12}Ti_{0.88}P$	670.3(6)	355.0(2)	812.9(5)	0.1934(4)
"$Hf_{1.2}Ti_{0.8}P$"	$Hf_{1.23}Ti_{0.77}P$	673.4(6)	355.4(2)	815.9(8)	0.1953(5)

Crystal Structure Studies of $Hf_{1-\delta}M_{1+\delta}As$

From each of the reactions (**I**), (**III**), (**IV**), and (**VI**), one single crystal was selected for structure refinements, to prove the formation of the Co_2Si type and to analyze the occupancy factors. Based on the powder data, the products were at the phase range borders; thus, determining their Hf/M ratios will give the phase width.

A Smart Apex CCD diffractometer (Bruker) using Mo-K_α radiation was employed for the data collections. In all four cases, 606 frames were collected with 0.3° scans in ω for exposure times of 60 seconds per frame. The data were corrected for Lorentz and Polarization effects. The unit cell dimensions and the systematic absences were consistent with the space group *Pnma* (and its noncentrosymmetric subgroup $Pn2_1a$), which is the space group of the Co_2Si type. This was subsequently confirmed by the successful structure refinements using SHELXL[36] yielding satisfying residual factors. Refining the structures in the noncentrosymmetric subgroup $Pn2_1a$ did not yield significant changes, but instead resulted in high correlations.

The Co_2Si type comprises three crystallographically independent atom sites (all on a mirror plane, Wyckoff notation 4*c*). The Si site was treated as the As site, and the two metal atom sites [denoted as M(1) and M(2)] were refined as being mixed occupied by Hf and M (Ti and V, respectively), with the sums of the occupancy factors fixed at 100%. M(1) is the Ti site in TiNiSi, and the Hf site in isostructural HfCoAs.[21]

In each case investigated here, the M(1) site was mainly occupied with Hf atoms, but exhibited always some Ti or V content. The M(2) site was either mixed occupied (with Hf as the minor component), or solely a Ti/V site, namely on the Hf-poor side of the phase range. Furthermore, the Hf contents of M(2) on the Hf-rich side [0.022(5) and 0.018(5)] may be regarded as insignificant. The refined formulas were $Hf_{0.84(1)}Ti_{1.16}As$, $Hf_{0.602(5)}Ti_{1.40}As$, $Hf_{0.97(2)}V_{1.03}As$, and $Hf_{0.916(6)}V_{1.084}As$, respectively. Crystallographic details are given in the Table 4. Atomic positions, occupancy factors, and displacement parameters are listed in Table 5. Further details of the crystal structure investigations can be obtained from the Fachinformationzentrum Karlsruhe, 76344 Eggenstein-Leopoldshafen, Germany, on quoting the depository numbers CSD-413262, -413263, -413264 and -413265.

Table 5. Atomic coordinates and equivalent displacement parameters [$pm^2 \times 10^{-1}$] of $Hf_{1-\delta}M_{1+\delta}As$

Atom[a]	*x*	*z*	$U_{eq.}$	Occupancy
M(1)[b]	0.4575(1)	0.6660(1)	4.7(3)	0.820(9) Hf, 0.180 Ti
M(1)[c]	0.4567(1)	0.6665(1)	6.3(3)	0.602(5) Hf, 0.398 Ti
M(1)[d]	0.4564(1)	0.6670(1)	6.6(3)	0.95(1) Hf, 0.05 V
M(1)[f]	0.45633(7)	0.66738(6)	5.1(2)	0.916(6) Hf, 0.084 V
M(2)[b]	0.3665(4)	0.0594(4)	4(1)	0.022(5) Hf, 0.978 Ti
M(2)[c]	0.3666(4)	0.0598(3)	5.2(6)	1 Ti
M(2)[d]	0.3720(5)	0.0578(4)	5(1)	0.018(5) Hf, 0.982 V
M(2)[e]	0.3714(3)	0.0581(2)	5.6(4)	1 V
As[b]	0.2438(3)	0.3589(2)	4.5(6)	1 As
As[c]	0.2456(2)	0.3593(2)	6.6(4)	1 As
As[d]	0.2428(3)	0.3607(3)	7.1(7)	1 As
As[e]	0.2432(2)	0.3600(1)	4.9(3)	1 As

[a] All atoms located on Wyckoff site 4*c*, with $y = 1/4$. [b] $Hf_{0.84(1)}Ti_{1.16}As$. [c] $Hf_{0.602(5)}Ti_{1.40}As$. [d] $Hf_{0.97(2)}V_{1.03}As$. [f] $Hf_{0.916(6)}V_{1.084}As$.

Electronic Structure Calculations

The band structures were calculated employing the self-consistent tight-binding *first principles* LMTO approximations (LMTO = linear muffin tin orbitals[37,38]). In the LMTO approach, the density functional theory is used with the local density approximation (LDA).[39] The integration in *k* space was performed by an improved tetrahedron method[40] on grids of 462 irreducible *k* points of the first Brillouin zone. Void space was filled with four so-called empty spheres. As structure models, we chose the structural parameters obtained from the refinements of $Hf_{0.84}Ti_{1.16}As$ and $Hf_{0.97}V_{1.03}As$ (using Hf parameters for M(1) and Ti and V parameters for M(2), respectively).

Table 4. Crystal data and structure refinements

Empirical formula	$Hf_{0.84}Ti_{1.16}As$	$Hf_{0.60}Ti_{1.40}As$	$Hf_{0.97}V_{1.03}As$	$Hf_{0.92}V_{1.08}As$
Molecular mass [g/mol]	280.74	249.34	300.52	293.83
Temperature [K]	293(2)	293(2)	293(2)	293(2)
Wavelength [pm]	71.073	71.073	71.073	71.073
Space group	*Pnma*	*Pnma*	*Pnma*	*Pnma*
Cell dimensions, *a* [pm]	684.3(2)	680.5(2)	674.1(2)	669.7(1)
b [pm]	361.34(7)	360.41(8)	358.88(9)	357.06(6)
c [pm]	832.2(2)	829.3(2)	807.3(2)	802.1(1)
V [nm^3]	0.20577(7)	0.20339(8)	0.19530(9)	0.19180(5)
No. of formula units per cell	4	4	4	4
Calculated density [mg/m^3]	9.06	8.14	10.22	10.18
Absorp. coeff. [mm^{-1}]	62.4	51.8	72.7	71.5
F(000)	477	428	506	496
Crystal size [μm]	50 × 45 × 20	42 × 39 × 14	44 × 42 × 20	49 × 45 × 14
Theta range	3.86−29.99°	3.87−33.13°	3.94−29.99°	3.96−35.01°
Reflections collected	796	949	733	791
Independent reflections (R_{int})	331 (0.032)	415 (0.078)	316 (0.034)	424 (0.022)
Absorption correction	sadabs	sadabs	sadabs	sadabs
Max. and min. transmission	1.00−0.60	1.00−0.61	1.00−0.69	1.00−0.74
Goodness-of-fit on F^2	1.213	0.901	1.358	1.129
$R(F)$, $R_w(F^2)$ (obsd. data)	0.043, 0.098	0.044, 0.083	0.047, 0.091	0.034, 0.075
$R(F)$, $R_w(F^2)$ (all data)	0.049, 0.100	0.061, 0.088	0.054, 0.093	0.038, 0.077
Extinction coefficient	0.0000(9)	0.0000(6)	0.0017(8)	0.0009(6)
Max. diff. peak, hole [e/$Å^3$]	6.09, −3.07	5.06, −2.86	3.43, −3.32	3.30, −3.25

Acknowledgments

Financial support from NSERC, CFI, OIT (Ontario Distinguished Researcher Award for H. K.), the Province of Ontario (Premier's Research Excellence Award for H. K.) and the Canada Research Chair program (CRC for H. K.) is appreciated.

[1] C. B. Shoemaker, D. P. Shoemaker, *Acta Crystallogr.* **1965**, *18*, 900−905.
[2] I. R. Mokra, O. I. Bodak, *Dopov. Akad. Nauk Ukrain. RSR* **1979**, 312−315.
[3] H. Kleinke, B. Harbrecht, *Z. Anorg. Allg. Chem.* **2000**, *626*, 1851−1853.
[4] J. C. Slater, *J. Chem. Phys.* **1964**, *41*, 3199−3204.
[5] D. G. Pettifor, *Solid State Commun.* **1984**, *51*, 31−34.
[6] P. Villars, *J. Less-Commun. Met.* **1983**, *92*, 215−238.
[7] C.-S. Lee, E. Dashjav, H. Kleinke, *Chem. Mater.* **2001**, *13*, 4053−4057.
[8] E. Dashjav, C.-S. Lee, H. Kleinke, *J. Solid State Chem.* **2002**, *169*, 96−102.
[9] G. Örlygsson, M. Conrad, B. Harbrecht, *Z. Anorg. Allg. Chem.* **2001**, *627*, 1017−1022.
[10] C.-S. Lee, E. Dashjav, H. Kleinke, *J. Alloys Comp.* **2002**, *338*, 60−68.
[11] S. Derakhshan, E. Dashjav, H. Kleinke, *Mat. Res. Soc., Symp. Proc.* **2002**, *755*, 341−346.
[12] Y. F. Lomnytska, Y. B. Kuz′ma, *J. Alloys Comp.* **1998**, *269*, 133−137.
[13] Y. F. Lomnitskaya, M. S. Brilyak, Y. B. Kuz′ma, *Neorg. Mater.* **1992**, *28*, 373−377.
[14] G. A. Marking, H. F. Franzen, *J. Alloys Comp.* **1994**, *204*, L17−L20.
[15] R. Berger, L. E. Tergenius, *Acta Chem. Scand., Ser. A* **1976**, *30*, 387−389.
[16] Y. Wang, L. D. Calvert, J. B. Taylor, *Acta Crystallogr., Sect. B* **1980**, *36*, 220−221.
[17] E. Garcia, J. D. Corbett, *J. Solid State Chem.* **1988**, *73*, 440−451.
[18] S. Rundqvist, P. C. Nawapong, *Acta Chem. Scand.* **1966**, *20*, 2250−2254.
[19] N. Chaichit, P. Chalugune, S. Rukvichai, P. Choosang, V. Kaewchansilp, C.-A. Pontchour, P. Phavanantha, *Acta Chem. Scand., Ser. A* **1978**, *32*, 309−311.
[20] H. Kleinke, H. F. Franzen, *Z. Anorg. Allg. Chem.* **1996**, *622*, 1893−1900.
[21] H. Kleinke, H. F. Franzen, *Z. Anorg. Allg. Chem.* **1998**, *624*, 51−56.
[22] H. Kleinke, C. Felser, *J. Solid State Chem.* **1999**, *144*, 330−338.
[23] H. Kleinke, *Z. Anorg. Allg. Chem.* **1998**, *624*, 1272−1278.
[24] Y. B. Kuz′ma, J. Y. Pivan, *Russ. J. Inorg. Chem.* **1979**, *24*, 1421.
[25] G. J. Miller, J. Cheng, *Inorg. Chem.* **1995**, *34*, 2962−2968.
[26] R. Hoffmann, *J. Chem. Phys.* **1963**, *39*, 1397−1412.
[27] M.-H. Whangbo, R. Hoffmann, *J. Am. Chem. Soc.* **1978**, *100*, 6093−6098.
[28] L. Pauling, *The Nature of the Chemical Bond*; 3rd ed.; Cornell University Press: Ithaca, New York, **1948**.
[29] X. Yao, G. Marking, H. F. Franzen, *Ber. Bunsenges.* **1992**, *96*, 1552−1557.
[30] M. Köckerling, H. F. Franzen, *Croat. Chem. Acta* **1995**, *68*, 709−719.
[31] H. Kleinke, *Inorg. Chem.* **1999**, *38*, 2931−2935.
[32] H. Kleinke, *Chem. Commun. (Cambridge)* **1998**, 2219−2220.
[33] H. Kleinke, *J. Mater. Chem.* **1999**, *9*, 2703−2708.
[34] H. Kleinke, *J. Am. Chem. Soc.* **2000**, *122*, 853−860.
[35] R. Dronskowski, P. E. Blöchl, *J. Phys. Chem.* **1993**, *97*, 8617−8624.
[36] G. M. Sheldrick, *SHELXTL*; Version 5.12 ed.; Siemens Analytical X-ray Systems: Madison, WI, **1995**.
[37] O. K. Andersen, *Phys. Rev. B* **1975**, *12*, 3060−3083.
[38] H. L. Skriver, *The LMTO Method*; Springer: Berlin, **1984**.
[39] L. Hedin, B. I. Lundqvist, *J. Phys. C* **1971**, *4*, 2064−2083.
[40] P. E. Blöchl, O. Jepsen, O. K. Andersen, *Phys. Rev. B* **1994**, *49*, 16223−16233.

Received July 16, 2003
Early View Article
Published Online February 10, 2004

